https://doi.org/10.26599/FRICT.2026.9441229

Research Article

Anomalous temperature-dependent friction in diamond-like carbon

Wen Wang[1,2,*], Wenjie He[1], Jiaming He[1], Xiao Huang[1], Junhui Sun[1], Qiang He[2], Yang Wang[1], Linmao Qian[1]

[1] School of Mechanical Engineering, Southwest Jiaotong University, Chengdu 610031, China

[2] Sichuan Key Technology Engineering Research Center for All-electric Navigable Aircraft, Sichuan Guanghan 618307, China

*Email: wangwen@swjtu.edu.cn

Received: April 16, 2025; Revised: November 25, 2025; Accepted: January 27, 2026

Abstracts

Due to the outstanding tribological and wear properties at cryogenic temperatures, Diamond-Like Carbon (DLC) materials are widely used in fields such as deep space exploration and superconducting magnets. Wherein, the temperature dependent frictional behavior of DLC is expected to follow the conventional thermally activated process. In this article, the frictional properties of DLC are scrutinized in the

temperature range of 300 to 100 K by reciprocally scanning a DLC coated atomic force microscopy (AFM) tip against a DLC substrate in ultra-high vacuum (UHV) conditions. The results reveal a remarkable monotonical temperature dependence of frictional behavior, which remains robust under varying normal loads and sliding velocities. Specially, the overall friction force raises as temperature decreases, with a distinct friction peak at T_{max} = 215 ± 10 K. While a logarithmic dependence of friction on velocity is observed at temperatures far from T_{max}, friction becomes nearly velocity-independent in the vicinity of T_{max}. This non-monotonically temperature dependence of friction beyond conventional thermally activated framework is well interpreted involving the formation/rupture of interfacial bonds. This work provides new insights into the interfacial bonding mechanisms affecting the tribological properties of DLC materials at cryogenic temperatures.

Keywords

Friction, UHV conditions, Cryogenic temperatures, DLC

1. Introduction

Solid lubricants are the inevitable option for interfacial lubrication of moving mechanical components at cryogenic/high temperatures or vacuum conditions, where the viscosity of fluid lubricants is significantly enhanced and even solidification. Attributable to the extraordinary low friction force, low wear rate and more provocative the multifunctionality of chemical and structural characteristics, DLC materials are one of the most widely utilized solid lubricants under the aforementioned extreme working conditions [1], [2]. From an application perspective, previous studies on the tribological properties of DLC films have essentially engaged in the macroscopic lubrication mechanism. The impacts of isolated variables, e.g. the formation of transfer layer and graphitization, wear progression, crack inception and thermal stability at elevated temperatures [3], [4], [5], [6] have been extensively probed. However, the interplay of these factors at different temperatures complicities mechanistic interpretation of DLC friction

behavior, hindering practical implementation [7].

As an example, the microscale friction measurements demonstrate that the friction coefficient (COF) of DLC based multilayer coatings increases monotonically when the sample temperature decreases from 25°C to -100°C [8]. Later studies reveals that the DLC film can maintain a superlubricity state even when the sample cools to -40°C, after which, considerable fluctuations in friction force arise as a consequence of competing factors like graphitization, wear initiation and transfer film formation, etc. [9]. Recent results suggest that the COF of DLC increases with the decrease of temperature, attributed to the reduced hydrogen passivation [10], [11]. The variability in outcomes stems from the fact that cryogenic temperature promotes crack nucleation and coating delamination during sliding. Although numerous studies have been conducted on the macroscopic frictional properties of DLC materials at cryogenic temperature for the purpose of application, the microscopic lubrication mechanisms remains scientifically intriguing and largely uncharted.

Generally, the micro/nanoscale frictional dynamics between solid surfaces is thermally activated process. In this process, thermal excitation endows extra energy to overcome the local sliding energy barrier. Accordingly, the classical thermal activation frictional theory trends toward predicting that the friction force gradually and monotonically increases with the decrease of temperature and typically follow the conventional Prandtl-Tomlinson (PT) model across a wide temperature range. Especially, the PT model agrees better with experimental data in the cryogenic regime. Intriguingly, recent results [11], [12], [13], [14] have revealed a nonmonotonic variation of dry nanoscale friction at cryogenic temperatures, which stems from the competing processes between the thermally activated formation/rupture of two bond types in the sliding interface. DLC is a class of carbon-based materials that exists in diverse phases, with varying fractions of $C(sp^3)$-$C(sp^3)$ bonds and $C(sp^2)$-$C(sp^2)$ bonds. Consequently, bonds formation/rupture process trends to dominant the frictional behavior at different temperatures, which remains experimentally unverified.

In this article, we present nanoscale AFM friction experiments in ta-C DLC/DLC interface as a function of temperature (100 K - 300 K), where both the sliding velocity v as well as the external applied

normal force F_N are varied systematically. Friction force shows a non-monotonic temperature dependence with a clear distinct friction peak at $T_{max} = 215 \pm 10$ K, which challenges the conventional PT model. By performing a systematic analysis with regard to the influence of v and F_N, our experiments thereby demonstrate that the peak temperature is unaffected by F_N but slightly increases with v, besides, the peak height decreases with F_N and v while the peak width stays nearly constant. By incorporating the multiple bonds formation/rupture theoretical framework, we reveal that the formation/rupture of the interfacial bonds dominates the frictional properties. This study allows for comparing the tribological behavior of DLC at different cryogenic temperatures under UHV conditions, which is essential for the further application of DLC under extreme conditions.

2. Experimental Approach

We selected ta-C as our sample since it has been widely used as solid lubricant under extreme conditions due to its long-time stability and smooth operation[15], [16]. In order to acquire a clean surface for the friction force measurements, the DLC sample was degassed at 453 K for 2 h in the UHV chamber to remove physical adsorbates and water layers. To study the effects of temperature on the nanoscale friction in the ta-C/ta-C interface, a commercial AFM cantilever (ContDLC from BudgetSensors, bending stiffness is 0.19 N/m) with a DLC coated tip was utilized in all measurements. The sample and AFM tip were assembled in a variable-temperature atomic force microscope (VT-AFM, ScientaOmicron) under UHV conditions, as illustrated in Fig. 1(a). We first cooled the DLC sample to a preset temperature and then waited for at least 2 hours with the aim of diminish the thermal drift caused by the temperature variation. Additionally, we normally waited for several minutes after the tip contacting with the cooled DLC surface. The lateral forces were carefully calibrated by exploiting the scanner tube's bending deformation during large-size scans, which sets up a correlation between the torsional stiffness and the bending stiffness of the rectangle cantilever [17]. An exemplary topography image of the degassed DLC surface (50 nm × 50 nm), captured at $T = 205.0 \pm 0.1$ K under a applied normal force of 6.8 nN and a scan velocity of 50 nm/s, is presented in Fig. 1(b). We then evaluated the surface roughness of DLC to be RMS

≈ 0.21 ± 0.04 nm. Fig. 1(c) display a typical height cross-sectional line affiliated with the black line in Fig. 1(b). In general, as a consequence of the intrinsic amorphous structure of DLC surface, the measured friction forces even by using the same AFM tip may vary with individual regions and also scan sizes. To obtain stable and intrinsic friction forces, a fixed scan area of 50 nm × 50 nm was used unless otherwise specified (See Figure S1 in SM for more information).

Fig. 1(d) plots the representative lateral force curves during the friction force measurements. More precisely, the red solid line (F_r) was acquired during the scanning from right (x = 50 nm) to left (x = 0 nm) while the blue one (F_t) was recorded in the opposite direction, as indicated by the red and blue horizontal arrows respectively. We can thereby calculate the friction force as $F = (< F_r > - < F_t >)/2$. To quantitatively probe the friction properties and minimize experimental errors, for each set of parameters, three independent friction measurements were carried out in different regions, and thus each data point in the article was determined from the average value.

Initially, the tip was sharp and not stable. Before starting the friction force measurements, we performed a pre-scan procedure on the DLC surface for 0.5 hours using a normal force of 20 nN and a scan velocity of 500 nm/s. Through this pre-scan procedure, a stable tip configuration was reached. At the onset of experiment, the adhesion force between the DLC tip and DLC substrate was 6.8 ± 0.5 nN. After 0.5 hours pre-scan, the adhesion force increased slightly to 10.2 ± 0.7 nN. This small change in the tip configuration is consistent with the fact that ta-C exhibits exceptionally high wear resistance (See Figure S5 in SM for more information). Subsequently, the same AFM cantilever was used throughout the friction measurements. To prevent damage and wear to both tip and sample, we maintained small normal forces of less than 17.7 nN throughout all measurements. During subsequent friction measurements, no obvious changes in the adhesion force were noticed at the same temperature, confirming that the tip was stable in the entire measurement (See Figure S2 in SM for more information).

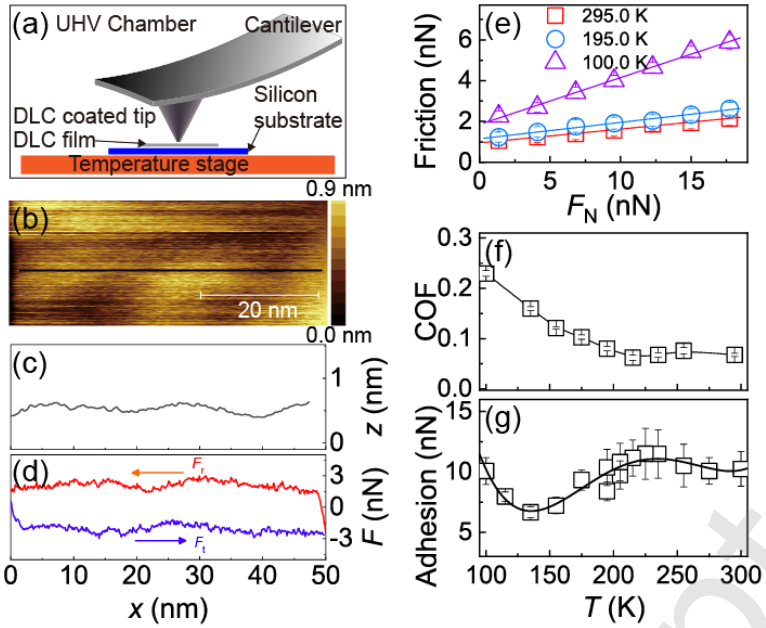

Fig. 1 Experimental details for nanoscale friction measurements and temperature effects on the friction force and adhesion force between the DLC tip and DLC substrate. (a) Graphic demonstration of the experimental system for friction measurements at various temperatures under UHV conditions ($p \leq 4 \times 10^{-10}$ mbar). (b) Typical AFM topography image recorded at $T = 205.0 \pm 0.1$ K with the external applied normal force of 6.8 nN and scan velocity of 50 nm/s. (c) A typical cross-sectional height profile affiliated with the black line marked in Fig. 1(b). (d) Representative recorded lateral force curves, where the red line (F_r) is the retrace scan while the blue one (F_t) is the trace scan. (e) Friction force shows a linear dependence on the externally applied normal force. (f) Temperature effects on COF. (g) Temperature dependence of adhesion force.

3. Results and discussion

To better perceive the frictional properties on DLC surface, one of the notable topics is how friction force F_f is influenced by temperature and normal force. Fig. 1(e) plots exemplary friction forces as a function of normal load at three temperatures, demonstrating a linear dependence, which indicates that the increase of friction with F_N is associated with the increase of real contact area. With the purpose of

evaluating the COF, which is little affected by probable tip configuration variations and/or adhesion changes, we carried out a linear fit to normal load-friction force data for each temperature (Fig. 1(e)). The evaluated COFs are hence plotted as a function of temperature in Fig. 1(f), ranging from 0.06 to 0.23. These values are equivalent to macroscopic measured COFs on DLC [18], [19], [20]. At this stage it is also fascinating to mention that the overall COF remains nearly invariant before T_{max} = 215 ± 10 K and then continuously increases with the decrease of temperature. The continuous increase of COF as temperature decreases is consistent with the previous results [8], [10], [11]. Fig. 1(g) presents the measured adhesion force as a function of temperature, indicating a nonlinear dependence.

We then focus on the temperature effects on friction. Fig. 2(a) plots 6 friction results at different temperature obtained with normal forces from 1.4 nN to 15.0 nN and velocity v = 500 nm/s. Across the normal forces range, a systematic increase of friction with decreasing temperature was observed. This observation is well in line with the framework of thermally activated friction [21], [22]. In addition to this, friction force at all temperatures increases with the normal force. Notably, an additional friction peak can be recognized for each normal load around the temperature between ~175 K and ~250 K (Fig. 2(a)), where a straight comparison of all peaks is provided in the upper panel of Fig. 2(a).

A closer inspection of the friction peak can thereby be done on the basis of peak fits [23] as manifest by the purple dashed line in the upper panel of Fig. 2(a). To quantitively manifest the impact of normal force on the friction peak, we define T_{max} as the temperature at the maximum friction, FWHM as the full width at half maximum of the friction peak, ΔF as the absolute height of the friction peak and $\Delta F/F_0$ as the relative friction peak height. These variables can be extracted though the peak fits, as schematically indicated in the upper panel of Fig. 2(a). The results of these variables are plotted in Fig. 2(b)-(e). The straight solid lines in Figs. 2(b)-(e) signify the overall trends of the load dependence: while the T_{max} and the FWHM holds virtually constant to the normal load, the ΔF and $\Delta F/F_0$ decrease linearly with F_N.

Finally, we measured the velocity effects on friction at different temperatures. More specifically, we performed velocity dependent measurements with changing sliding velocities from 50 nm/s to 10000 nm/s at a fixed normal force of 6.8 nN for 13 different temperatures. Three exemplary results for temperatures

at T = 300.0 K, T = 195.0 K, and T = 100.0 K are plotted in Figs. 3(a)-(c). In all instances, the velocity dependence of friction follows a logarithmic trend, as indicated by the straight solid lines.

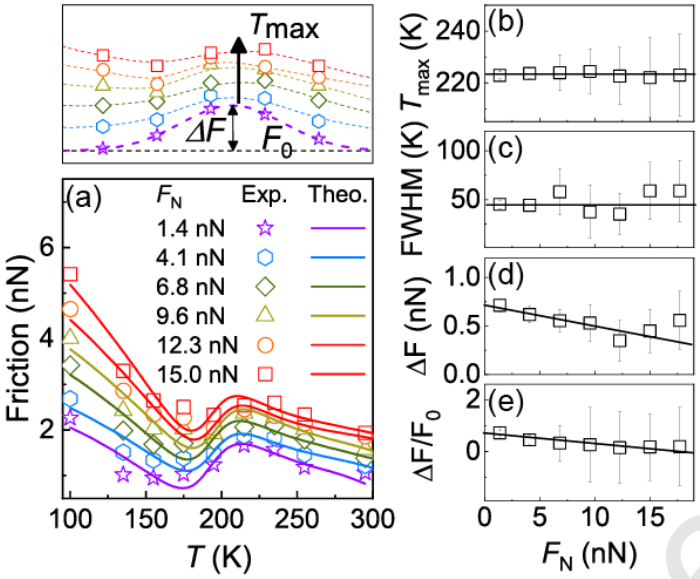

Fig. 2 Temperature and normal load effects on friction force. (a) The recorded friction force as a function of temperature at different normal loads (lower panel), where the solid lines are theoretical curves. Straight comparison of all friction peaks from 160 K to 275 K is additionally shown in the upper panel. The vertical black arrow manifests the increase of the normal force direction. (b) T_{max}, (c) FWHM, (d) ΔF and (e) $\Delta F/F_0$ as a function of normal force.

Nevertheless, distinct differences in the semi-logarithmic plot slopes can be obviously detected. Positive slopes, as expected based on the concept of thermally activated friction [21], [22], are observed for the two temperatures (i.e. T = 300.0 K and T = 100.0 K) away from T_{max}, while zero or even negative slopes are evident in Fig. 3(b) in the vicinity of T_{max}. This contrast is furthermore emphasized by Fig. 3(d), which shows all semi-logarithmic plot slopes versus temperature. The slope decreases with the decrease of temperature before ~ 240 ± 10 K, then remains nearly invariant to temperature between 150.0 K and 240.0 K, and finally increases with the further decrease of temperature. These slopes are generally positive and only become nearly zero or negative in the temperature range of 150.0 K - 240.0 K, which indicates a fundamental change of the energy dissipation mechanism.

On the basis of the same data-set, we then scrutinized the temperature-dependent friction data for different sliding velocities as exemplified by Fig. 4(a) for sliding velocities of v = 50 nm/s and v = 5000 nm/s. Once more, the velocity dependence of T_{max}, FWHM, ΔF, and $\Delta F/F_0$ are plotted in Figs. 4(b)-(e). We notice that T_{max} (Fig.4(b) moderately increases with sliding velocity and FWHM ≈ 65 ± 5 K again stays generally constant, while both ΔF (Fig.4(d) and $\Delta F/F_0$ (Fig. 4(e) decrease logarithmically with the sliding velocity v.

Previous friction force measurements on diverse substrates including HOPG, Si, NaCl, etc. have unveiled that friction changes non-monotonically with temperature [24], [25], [26], [27], which are analogous to the results presented in Figs. 2 and 4. Kinetic Monte Carlo simulations [28] and multi-contact theoretical models [12], [29] have revealed that the mechanism of unanticipated temperature dependence of friction is originated from the formation/rupture of interfacial strong and weak bonds. Within this framework, the velocity dependence of friction also varies with temperature [30]. The variation of adhesion force (Fig. 1(g)) additionally manifests the change of the tip- substrate interaction. Since both the DLC substrate and the DLC tip contains a large amount of free dangling bonds, the interfacial bonds formation/rupture during relative sliding is crucial in determining the frictional behavior[31], [32] (See Figure S3 and S4 in SM for more information).

We turn to the theoretical approach to understand the effects of multiple bonds formation/rupture on friction [14], [30], [33]. The overall friction force is expressed as $F = F^{\mathrm{I}} + F^{\mathrm{II}}$. Superscripts i = I and II represent the strong and weak bonds within the interface, respectively. The friction force resulted from a single type of bond F^i is analytical expressed as [14], [30]:

$$F^i = N^i \frac{k_B T}{x_s} \frac{r_{on}(\sigma_0) B^i e^{B^i} Q(B^i)}{1 + r_{on}(\sigma_0) B^i e^{B^i} E_1(B^i)} \qquad (1)$$

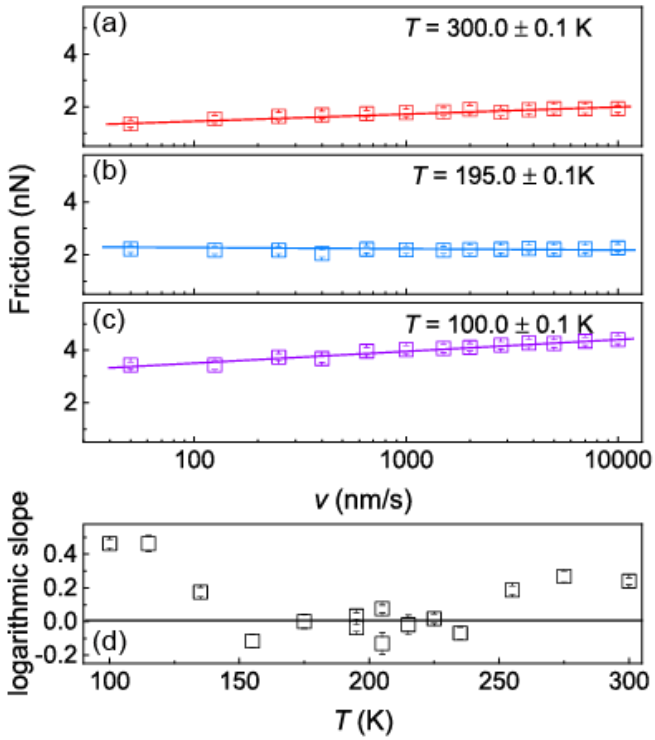

Fig. 3 Temperature and normal load effects on friction force. (a) The recorded friction force as a function of temperature at different normal loads (lower panel), where the solid lines are theoretical curves. Straight comparison of all friction peaks from 160 K to 275 K is additionally shown in the upper panel. The vertical black arrow manifests the increase of the normal force direction. (b) T_{max}, (c) FWHM, (d) ΔF and (e) $\Delta F/F_0$ as a function of normal force.

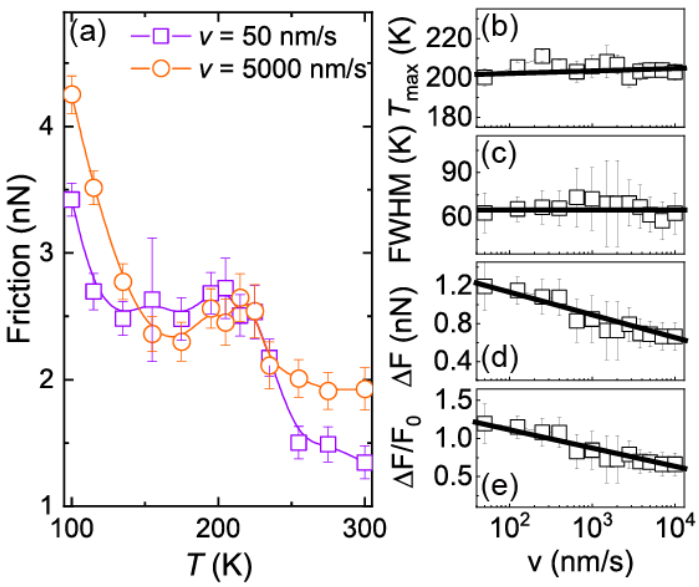

Fig. 4 Temperature and normal load effects on friction force. (a) The recorded friction force as a function of temperature at different normal loads (lower panel), where the solid lines are theoretical curves. Straight comparison of all friction peaks from 160 K to 275 K is additionally shown in the upper panel. The vertical black arrow manifests the increase of the normal force direction. (b) T_{max}, (c) FWHM, (d) ΔF and (e) $\Delta F/F_0$ as a function of normal force.

Here, N is the number of interfacial bonds, x_s = 0.032 nm is the distance between the minimum and saddle point in the potential landscape [14]. $\sigma_0 = 3(F_N + F_a)/(2\pi a^2)$ represents the maximum normal stress in the center of tip, $a = (3R(F_N + F_a)/4E^*)^{1/3}$ is the contact radius obtained by using the Hertzian contact model, $E^* = \dfrac{E}{2(1-\nu^2)}$ is the effective Young's modulus. The Young's modulus and Poisson's ratio for the DLC substrate and the DLC tip are E = 759 GPa and μ = 0.17 [34]. In order to account for the temperature dependence of adhesion force, the adhesion force can be simply expressed as $F_a = 6.2\times10^{-8}\cdot T^4 - 5.5\times10^{-5}\cdot T^3 + 0.02\cdot T^2 - 2.3\cdot T + 115.75$ by fitting the adhesion data points as shown in Fig. 1(g) as a solid line. $r_{on} = (k_{on}^0/k_{off}^0)\exp[(\Delta E_{off} - \Delta E_{on})/k_B T]$ denotes the ratio between creating

and breaking interfacial bonds. $k_{\text{on}}^0 = k_{\text{off}}^0 = 10^{13}$ Hz is the attempting frequencies for bonds formation and rupture. $\Delta E_{\text{on}} = E_{\text{on}} - \sigma_0 V_{\text{on}}$ and $\Delta E_{\text{off}} = E_{\text{off}} - \sigma_0 V_{\text{off}}$ are the barrier heights for creating bonds and breaking bonds with V_{on} and V_{off} representing the activation volume. $B = (k_B T / \kappa_b x_s v) k_{\text{off}}^0 \exp(-\Delta E_{\text{off}} / k_B T)$, $E_1(B) = \int_B^\infty \frac{e^{-x}}{x} dx$ and $Q(B) = \int_1^\infty \frac{\ln(x)}{x} e^{-Bx} dx$ [14], [30], [33].

We then used Eq. (1) to fit the temperature dependence of friction force by fixing the tip radius to R= 15 nm. The fitted results are then plotted in Fig. 2(a) as solid lines. Consistent with experimental observations, friction force increases firstly then decreases and finally increases again. The fitting parameters are $E_{\text{on}}^{\text{I}} = 0.50 \pm 0.01$ eV, $E_{\text{off}}^{\text{I}} = 1.37 \pm 0.21$ eV, $N^{\text{I}} = 2 \pm 1$, $V_{\text{on}}^{\text{I}} = 1.0 \pm 0.1$ Å^3, $V_{\text{off}}^{\text{I}} = 5.3 \pm 4.3$ Å^3, $E_{\text{on}}^{\text{II}} = 0.10 \pm 0.01$ eV, $E_{\text{off}}^{\text{II}} = 0.44 \pm 0.02$ eV, $N_{\text{II}} = 7 \pm 2$, $V_{\text{on}}^{\text{II}} = 7.3 \pm 2.7$ Å^3, $V_{\text{off}}^{\text{I}} = 1.0 \pm 0.1$ Å^3. The errors represent the standard deviation among different fits at different normal forces. Within the multi-bond formation/rupture theoretical framework, the bond number is treated as primarily constant since it is assumed to be determined by contact area. The bond numbers may vary with temperature, however this represents an important and complex phenomenon that warrants dedicated theoretical and experimental investigation in future works.

The reported interfacial bond density falls within the range of $0.1/\text{nm}^2 \le n \le 10/\text{nm}^2$ [14], [30]. In our measurements, the AFM tip radius is approximately 15 nm. For a typical external normal load of 10 nN, the contact area is estimated using the Hertz contact model to be $A = \pi \left(\frac{3FR(1-\mu^2)}{2E} \right)^{2/3} = 1.4 \text{ nm}^2$, resulting in an estimated number of interface bonds ranging from 0.14 to 14. These values align well with the fitted results. Additionally, the remaining parameters are directly comparable to those reported in Ref. [30] and Ref. [14]. Notably, the energy barrier for creating a strong bond is 0.5 eV, derived from fitting the AFM experimental data. This value also falls within the expected range for formation of C-C bonds (0.4–0.8 eV) [35], [36]. Finally, our theoretical approach estimates an energy barrier of 1.37 eV for breaking the strong interfacial bond, which is consistent with the range of 1–4 eV reported for breaking carbon bonds in DLC [37].

Based on the multiple bonds formation/rupture model, the influence of velocity on the temperature-dependent behavior of friction (Fig.4 (a)) can be qualitatively explained. Only a few bonds can form during sliding in the cryogenic temperature regime. In contrast, the time-averaged friction force reaches its equilibrium value in the high temperature regime. Therefore, the formation and rupture of contacts play a minor role in determining the velocity dependence of friction in both the cryogenic and high temperature regimes and friction increases logarithmically with velocity as shown in Figs. 3(a) and (c). Whereas, unexpected velocity dependent behaviors (Fig. 3(b)) appear since the friction is dominated by formation/rupture of interfacial bonds in the moderate temperature regime. In this temperature regime, the overall number of bonds with higher energy barriers decreases with velocity, leading to that friction force decreases with velocity[14].

4. Conclusions

Inconclusion, our investigation is an extensive characterization of nanoscale friction on DLC under UHV conditions in a wide range of temperatures, velocities and normal forces. Our experiments reveal a distinct peak in friction at $T_{max} = 215 \pm 10$ K. The temperature of the friction peak is independent of the normal force and slightly increases with velocity. The width of friction peak remains invariant to normal force and velocity. The magnitude of the friction peak decreases with normal force and velocity. While logarithmic dependence of friction on velocity is observed far from T_{max} as expected based on the concept of thermally activated friction, a nearly constant friction is observed in the vicinity of T_{max}. The thermally activated and shear assisted formation/rupture of the interfacial bonds primaries the whole process. Our results reveal the frictional properties of DLC in UHV conditions in a systematic way, which may guide the application of DLC at cryogenic temperatures.

Acknowledgments

The authors gratefully acknowledge the financial support by the NSFC (Grant Nos. 12172309, 11890672, 61704013, 11602205, 52475220), NSFSC (GrantNos. 2022NSFSC1917,2023NSFSC1988),

Sichuan Science and Technology Program (No. 2021YFSY0017), Scientific Research and Innovation Projects of Central Universities (2682024ZTPY045), Shenzhen Key Laboratory of Superlubricity Technology (ZDSYS20230626091701002), Sichuan province all-electric navigation aircraft key technology engineering research center (Grant No. CAFUC202401KF007), the Analytical and Testing Center of Southwest Jiaotong University for the AFM measurements.

Declaration of competing interest

The authors have no competing interests to declare that are relevant to the content of this article.

References

[1] G. Theiler, W. Hübner, T. Gradt, P. Klein, K. Friedrich, Friction and wear of ptfe composites at cryogenic temperatures, Tribology international 35 (7) (2002) 449–458.

[2] C. Donnet, A. Erdemir, Tribology of diamond-like carbon films: fundamentals and applications, Springer Science & Business Media, 2007.

[3] X. Deng, H. Kousaka, T. Tokoroyama, N. Umehara, Tribological behavior of tetrahedral amorphous carbon (ta-c) coatings at elevated temperatures, Tribology international 75 (2014) 98–103.

[4] K. Al Mahmud, M. Varman, M. A. Kalam, H. H. Masjuki, H. Mobarak, N. Zulkifli, Tribological characteristics of amorphous hydrogenated (ac:H) and tetrahedral (ta-c) diamond-like carbon coating at different test temperatures in the presence of commercial lubricating oil, Surface and Coatings Technology 245 (2014) 133–147.

[5] A. Vahidi, F. Ferreira, J. Oliveira, Comparative study of dry high-temperature tribological performance of hydrogen-free and hydrogenated dlc films deposited by hipims in doms mode, Tribology International 195 (2024) 109639.

[6] Y. Wang, J. Xu, J. Zhang, Q. Chen, Y. Ootani, Y. Higuchi, N. Ozawa, J. M. Martin, K. Adachi, M. Kubo, Tribochemical reactions and graphitization of diamond-like carbon against alumina give

volcano-type temperature dependence of friction coefficients: A tight-binding quantum chemical molecular dynamics simulation, Carbon 133 (2018) 350–357.

[7] Y. L. Ostrovskaya, T. Yukhno, G. Gamulya, Y. V. Vvedenskij, V. Kuleba, Low temperature tribology at the b. verkin institute for low temperature physics & engineering (historical review), Tribology international 34 (4) (2001) 265–276.

[8] T. Ye, J. Ma, Z. Jia, T. Li, W. Liu, W. Yu, Microstructure, mechanical properties and low-temperature tribological behavior of cr/cr-w/w-dlc/dlc multilayer coatings on 5a06 al alloy, Journal of Materials Research and Technology 18 (2022) 810–819.

[9] Q. Ma, C. Huang, W. Cai, J. Zhang, W. Chen, J. Jin, Y. Xia, Y. Xu, T.Ma, Revealing the low-temperature friction behavior and mechanisms of hydrogenated amorphous carbon films with al/cr/si doping, Tribology International 198 (2024) 109911.

[10] M. Aggleton, J. Burton, P. Taborek, Cryogenic vacuum tribology of diamond and diamond-like carbon films, Journal of Applied Physics 106 (1) (2009).

[11] W. Chen, K. Wang, X. Miao, J. Zhang, A. Song, X. Chen, J. Luo, T. Ma, Ultralow-friction at cryogenic temperature induced by hydrogen correlated quantum effect, Small (2024) 2400083.

[12] A. Filippov, J. Klafter, M. Urbakh, Friction through dynamical formation and rupture of molecular bonds, Physical Review Letters 92 (13) (2004) 135503.

[13] I. Barel, M. Urbakh, L. Jansen, A. Schirmeisen, Multibond dynamics of nanoscale friction: the role of temperature, Physical Review Letters 104 (6) (2010) 066104.

[14] B. Hu, X. Zhou, W. Ouyang, W. Wang, Unconventional temperature dependence of friction at the single-asperity silicon/graphite interface, Physical Review B 110 (18) (2024) 184112.

[15] J. Robertson, Diamond-like amorphous carbon, Materials science and engineering: R: Reports 37 (4-6) (2002) 129–281.

[16] F. M. Elam, F.-C. Hsia, S. van Vliet, R. Bliem, L. Yang, B. Weber, S. E. Franklin, The influence of

corrosion on diamond-like carbon topography and friction at the nanoscale, Carbon 179 (2021) 590–599.

[17] W. Wang, D. Dietzel, A. Schirmeisen, Single-asperity sliding friction across the superconducting phase transition, Science advances 6 (12) (2020) eaay0165.

[18] F. Zhao, H. Li, L. Ji, Y. Wang, H. Zhou, J. Chen, Ti-dlc films with superior friction performance, Diamond and Related materials 19 (4) (2010) 342–349.

[19]B. Vengudusamy, R. A. Mufti, G. D. Lamb, J. H. Green, H. A. Spikes, Friction properties of dlc/dlc contacts in base oil, Tribology international 44 (7-8) (2011) 922–932.

[20] S. Jiadong, M. Guozheng, H. Cuihong, W. Haidou, L. Guolu, W. Aobo, L. Yunfan, Y. Qingsong, The tribological performance in vacuum of dlc coating treated with graphene spraying top layer, Diamond and Related Materials 125 (2022) 108998.

[21] E. Gnecco, R. Bennewitz, T. Gyalog, C. Loppacher, M. Bammerlin, E. Meyer, H. J. Güntherodt, Velocity dependence of atomic friction, Phys. Rev. Lett. 84 (6) (2000) 1172–1175.

[22] Y. Sang, M. Dubé, M. Grant, Thermal effects on atomic friction, Phys. Rev. Lett. 87 (17) (2001) 174301.

[23] W. Wang, D. Dietzel, C. Liu, A. Schirmeisen, Nanoscale friction across the first-order charge density wave phase transition of 1t-tas2, ACS Applied Materials & Interfaces 15 (3) (2023) 4774–4780.

[24] S. J. Manzi, W. T. Tysoe, O. J. Furlong, Temperature dependences in the tomlinson/prandtl model for atomic sliding friction, Tribology Letters 55 (2014) 363–369.

[25] Y. Zhang, M. Dong, B. Gueye, Z. Ni, Y. Wang, Y. Chen, Temperature effects on the friction characteristics of graphene, Applied Physics Letters 107 (1) (2015).

[26] C. Greiner, J. R. Felts, Z. Dai, W. P. King, R. W. Carpick, Controlling nanoscale friction through the competition between capillary adsorption and thermally activated sliding, ACS nano 6 (5) (2012) 4305–4313.

[27] I. Barel, M. Urbakh, L. Jansen, A. Schirmeisen, Temperature dependence of friction at the nanoscale: when the unexpected turns normal, Tribology letters 39 (2010) 311–319.

[28] Z. Li, L. Pastewka, I. Szlufarska, Chemical aging of large-scale randomly rough frictional contacts, Physical Review E 98 (2) (2018) 023001.

[29] Q. Li, T. E. Tullis, D. Goldsby, R. W. Carpick, Frictional ageing from interfacial bonding and the origins of rate and state friction, Nature 480 (7376) (2011) 233–236.

[30] W. Ouyang, Y. Cheng, M. Ma, M. Urbakh, Load-velocity-temperature relationship in frictional response of microscopic contacts, Journal of the Mechanics and Physics of Solids 137 (2020) 103880.

[31] Y. Wang, Y. Li, X. Huang, J. Xu, Y. Ootani, N. Ozawa, K. Adachi, L. Qian W. Wang, M Kubo, A generalized friction law depicting the thermal effects at chemical bonding interface. Friction, 2025, 13(6).

[32] Ouyang W, Ramakrishna S N, Rossi A, et al. Load and velocity dependence of friction mediated by dynamics of interfacial contacts. Physical Review Letters, 2019, 123(11): 116102.

[33] W. Wang, H. Lei, A. Wang, Temperature dependence of nanoscale friction on topological insulator bi2se3 surfaces, Nanotechnology 33 (39) (2022) 395706.

[34] S. Cho, I. Chasiotis, T. A. Friedmann, J. P. Sullivan, Young's modulus, poisson's ratio and failure properties of tetrahedral amorphous diamond-like carbon for mems devices, Journal of Micromechanics and Microengineering 15 (4) (2005) 728.

[35] Y. Liu, S. Müller, D. Berger, J. Jelic, K. Reuter, M. Tonigold, M. Sanchez-Sanchez, J. A. Lercher, Formation mechanism of the first carbon–carbon bond and the first olefin in the methanol conversion into hydrocarbons, Angewandte Chemie International Edition 55 (19) (2016) 5723–5726.

[36] J. M. Parr, M. R. Crimmin, Carbon–carbon bond activation by mg, al, and zn complexes, Chemical Science 14 (40) (2023) 11012–11021.

[37] S.Veprek, Recent search for new superhard materials: Go nano!, Journal of Vacuum Science &

Technology A 31 (5) (2013).